Chemical Engineering Science 149 (2016) 129–142

Contents lists available at ScienceDirect

Chemical Engineering Science

journal homepage: www.elsevier.com/locate/ces

Hydrodynamic effects on three phase micro-packed bed reactor performance – Gold–palladium catalysed benzyl alcohol oxidation

Noor Al-Rifai [a], Federico Galvanin [a], Moataz Morad [b], Enhong Cao [a], Stefano Cattaneo [b], Meenakshisundaram Sankar [b], Vivek Dua [a], Graham Hutchings [b], Asterios Gavriilidis [a,*]

[a] Department of Chemical Engineering, University College London, Torrington Place, London WC1E 7JE, UK
[b] Cardiff Catalysis Institute, School of Chemistry, Cardiff University, CF10 3AT, UK

HIGHLIGHTS

- Hydrodynamics influence the performance of Au–Pd catalysed benzyl alcohol oxidation in a micro-packed bed.
- Mass transfer enhancement is found in the gas-continuous flow regime.
- Benzaldehyde selectivity higher than a batch reactor is obtained at very high gas:liquid flow rate ratios.
- Flow regimes in three phase micro-packed beds differ from their macro-scale counterparts.
- A response surface model is able to locate the operating conditions for yield optimisation.

GRAPHICAL ABSTRACT

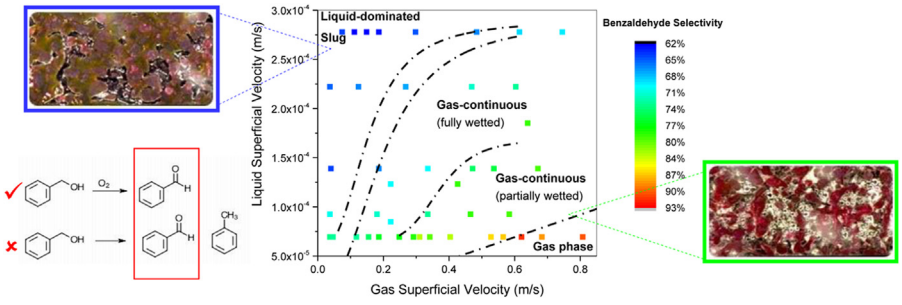

ARTICLE INFO

Article history:
Received 30 August 2015
Received in revised form
11 March 2016
Accepted 12 March 2016
Available online 26 March 2016

Keywords:
Multiphase microreactor
Hydrodynamics
Multiphase flow
Aerobic oxidation
Gold/palladium catalyst
Response surface methodology

ABSTRACT

The hydrodynamics of a three-phase micro-packed bed reactor and its effect on catalysed benzyl alcohol oxidation with pure oxygen were studied in a silicon–glass microstructured reactor. The microreactor was operated at 120 °C and 1 barg and contained a channel with a 300 μm × 600 μm cross-section, packed with 1 wt% Au–Pd/TiO_2 catalyst, 65 μm in average diameter. Improvements in the conversion of benzyl alcohol and selectivity to benzaldehyde were observed with increasing gas-to-liquid ratio, which coincided with a change in the flow pattern from a liquid-dominated slug to a gas-continuous flow regime. The observed enhancement is attributed to improved external mass transfer, associated with an increase in the gas–liquid interfacial area and reduction in the liquid film thickness that occur with gradual changes in the flow pattern. A maximum selectivity of 93% to benzaldehyde was obtained under partial wetting – which introduced the added benefit of direct gas–solid mass transfer – outperforming the selectivity in a conventional glass stirred reactor. However, this was at the expense of a reduction in the conversion. A response surface model was developed and then used to predict optimal operating conditions for maximum benzaldehyde yield, which were in the gas-continuous flow regime. This corresponded to relatively high gas flow rate in conjunction with moderate liquid flow rate, ensuring sufficient catalyst wetting with a thin film to reduce transport resistances.

1. Introduction

Alcohol oxidation to aldehydes is an important process in organic chemistry due to the significance of these products as high

* Corresponding author.
E-mail address: a.gavriilidis@ucl.ac.uk (A. Gavriilidis).

http://dx.doi.org/10.1016/j.ces.2016.03.018

value building block molecules for further manufacture into everyday consumer products. Developing clean and selective reactions is the latest paradigm in organic synthesis, underpinned by an effort to reduce the economic and environmental costs of chemical production. Catalytic methodologies are making way for greener, low cost processes, replacing traditional metal oxides that are responsible for environmentally damaging wastes and poor atom efficiencies. However, the presence of both gaseous and liquid reactants results in added complexity to the transport of reactants from their respective phases to the catalytic active sites. The characteristic times for transport processes can range between 10 and 10^{-3} s (Hessel et al., 2009) hence interference of these physical processes with reaction kinetics can limit the reaction performance significantly, affecting the observed activity and product selectivity. Complex interactions between the flowing fluid phases and the stationary solid particles lead to differing flow patterns that depend on a number of factors: packing density, gas and liquid velocities, particle size, and physical properties of the fluid phases (Ranade et al., 2011). Identification of the flow characteristics is central to understanding reactor behaviour due to their direct impact on other transport processes, such as heat and mass transfer around the catalyst.

Typically, the reactants in the gaseous and liquid phases diffuse through the boundary layer and into the catalyst pores before reacting. Fast reactions in particular are often limited by mass transfer steps and for partial oxidation reactions, the characteristic reaction time can be only a few milliseconds (the same order of magnitude as the physical processes), thus the reaction becomes highly dependent on parameters involving the diffusion behaviour between the gas and liquid phases, the size of the catalyst particle, the pore size diameter, physical properties of the fluids, and flow conditions of the gas and liquid reactants (Hessel et al., 2009).

The influence of the flow regime on reaction performance has been the subject of various trickle bed reactor studies. It has been demonstrated that an enhancement in reactor performance is possible while operating under pulsing flow (Wilhite et al., 2001) as well as externally forced cyclic operation (Khadilkar et al., 1999; Lange et al., 1999; Atta et al., 2014; Wilhite et al., 2003). The enhancement in mass transfer under pulsing flow was attributed to the strong interaction between the phases within the pulses and the periodic nature of the flow environment around the stationary catalyst. Most of these studies featured reactions where the gas-side mass transfer was not significantly influenced by the flow regime, owing to the assumption that the liquid phase is always saturated with gas (i.e. high gas solubility in the liquid phase). The influence of the hydrodynamics on reaction performance will therefore depend on which of the mass transfer steps governs the reaction rate.

The advent of micro-packed bed reactors as lab investigation tools for multiphase catalysis (Kockmann, 2008; Al-Rifai et al., 2013) spawned a burst of research into characterising and understanding their hydrodynamics (Faridkhou and Larachi, 2012, 2014; Iliuta et al., 2012; Moulijn et al., 2015; Faridkhou et al., 2013; Krishnamurthy and Peles, 2007; Losey et al., 2001; van Herk et al., 2005). Most efforts have been dedicated to the identification of differences from the macro-scale in relation to various parameters: liquid hold-up, pressure drop, porosity and flow regime transition. Deviations from what is commonly observed in macroscale reactors are expected due to a strong increase in the effect of capillary forces when scaling down reactor and particle size (Moulijn et al., 2015; Faridkhou et al., 2013). While the influence of gas and liquid flow rate on liquid holdup in micro-packed beds has been found to be similar to conventional reactors (Faridkhou and Larachi, 2012), the absolute value of the liquid holdup in micro-packed beds is under-predicted by conventional hydrodynamic models (Iliuta et al., 2012). Microscale reactors do not necessarily possess ideal behaviour, as the small particle diameter commonly used in these reactors leads to high capillary forces, resulting in liquid maldistribution and channelling (Moulijn et al., 2015). The high capillary pressures have been found to have adverse effects on the two-phase pressure drop, as well as a tendency to influence liquid spreading across the porous medium, where higher capillary forces cause the liquid phase to displace from the high porosity zone (wall) to the low porosity region (centre) (Iliuta et al., 2012). A more thorough discussion of the differences in behaviour between conventional and micro-scale reactors can be found elsewhere (Faridkhou et al., 2013).

1.1. The reaction: benzyl alcohol oxidation on Au–Pd/TiO_2

Benzyl alcohol oxidation is one of the most studied alcohol oxidation reactions due to the demand for benzaldehyde as an intermediate in the production of fine chemicals, pharmaceuticals, flavourings and fragrances. It has therefore been used as a model substrate for selective alcohol oxidations (Ferri et al., 2006; Choudhary and Dumbre, 2010; Yamaguchi and Mizuno, 2002).

In the solvent-free oxidation of benzyl alcohol on gold–palladium catalysts, two pathways have been identified as the source of the principal product benzaldehyde (Meenakshisundaram et al., 2010; Enache et al., 2006); (1) direct catalytic oxidation, yielding benzaldehyde exclusively and taking place in the presence of gaseous oxygen and (2) disproportionation to give equal amounts of benzaldehyde and a side product, toluene (Fig. 1).

The average turnover frequencies for the individual reactions: oxidation (TOF_O), disproportionation (TOF_D) and the overall reaction (TOF_T) can be quantified as previously demonstrated by Sankar et al. (2011). Toluene is formed exclusively from disproportionation, and therefore, the amount of toluene formed can be used as a measure of the extent of the disproportionation reaction. The average *TOF*s can be quantified using the following equations:

$$TOF_O = \frac{F_{PhCHO} - F_{PhCH_3}}{mol_{metal}} = \frac{F_{PhCH_2OH,0} \bullet C \bullet (S_{PhCHO} - S_{PhCH_3})}{mol_{metal}}$$

$$TOF_D = \frac{2 \bullet F_{PhCH_3}}{mol_{metal}} = \frac{2 \bullet F_{PhCH_2OH,0} \bullet C \bullet S_{PhCH_3}}{mol_{metal}}$$

$$TOF_T = \frac{F_{PhCH_2OH,0} \bullet C}{mol_{metal}}$$

The parallel reaction scheme presents both conversion and selectivity issues. There is strong evidence to suggest that catalyst design and reactor operating conditions are crucial in determining the relative extent of each reaction (Meenakshisundaram et al.,

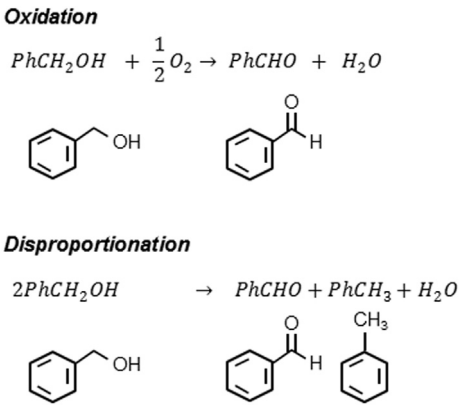

Fig. 1. Simplified benzyl alcohol oxidation reaction scheme.

2010; Cao et al., 2013). The global transformation rate can also be limited by transport phenomena and the relative importance of these transport phenomena is dictated by the chemical reaction kinetics. As a result, it is possible that the reaction performance is different compared to the performance attainable in the kinetic regime.

The focus of this work is two-fold: identification of flow patterns present in a micro-packed bed reactor, as well as mapping of these flow regimes and their dependence on gas and liquid flow conditions. Secondly, it is to assess the practical implications of these hydrodynamic changes, by studying their impact on the performance of Au–Pd/TiO_2 catalysed benzyl alcohol oxidation. A response surface model is built for a quantitative description of the reactor performance at different gas and liquid flow rates, providing predictions for the optimum reaction conditions within the investigated experimental region.

2. Materials and methods

2.1. Catalyst preparation method

The catalyst used was a 0.05 wt% Au–0.95 wt% Pd supported on titanium dioxide, prepared via an excess-anion modified impregnation method (Sankar et al., 2012). $HAuCl_4 \cdot 3H_2O$ (Sigma Aldrich) and solid $PdCl_2$ (Sigma Aldrich) were used as the metal precursors. For the typical synthesis of 2 g of this catalyst, 0.0319 g of $PdCl_2$ was dissolved in 1.66 ml of 0.58 M HCl. To this solution, 0.08 ml of gold solution (concentration 12.5 mg Au/ml) was added in a 50 ml round bottom flask, followed by a further 13 ml of double distilled water. The flask was then immersed into an oil bath placed on a magnetic stirrer hot plate. The solution was stirred vigorously at 1000 rpm and the temperature of the oil bath was raised from 27 °C to 60 °C till the Pd solid had completely dissolved. Then, at 60 °C, 1.98 g of the metal oxide support material TiO_2 (Degussa Evonik P25) was added slowly over a period of 8 to 10 min with constant stirring. After the completion of addition of the support material, the slurry was stirred at 60 °C for an additional 15 min. The temperature of the oil bath was then raised to 95 °C and the slurry was stirred at that temperature for a further 16 h until all the water evaporated, leaving a dry solid. The solid powder was ground thoroughly in a mortar and pestle to form a uniform mixture, 400 mg of which was transferred and spread out over a glass calcination boat (13 cm in length) placed in a calcination furnace fitted with inlet and outlet valves. The temperature of the furnace was raised from 30 °C to 400 °C at a heating rate of 10 K/min under a steady flow of 5% H_2 in Ar and kept at 400 °C for 4 h. Finally, the furnace was cooled over a period of 15 to 30 min and this "reduced" sample was used without any further treatment.

The BET surface area was analysed on a pre-pelletised catalyst using Quadrasorb evo™ Surface Area Analyzer and Pore Size Analyzer. Prior to the analysis of the sample, it was degassed in a FLOVAC Degasser at 200 °C for 2 h. The BET surface area of the material was found to be 65.3 m^2/g.

2.2. Micro-packed bed reactor (MPBR)

The silicon–glass microreactors used in this work were fabricated by photolithography and deep reactive ion etching and sealed via anodic bonding to glass, as described elsewhere (Cao et al., 2011). The serpentine microchannel dimensions were 600 μm (W) × 300 μm (H) × 190 mm (L). The gas was introduced into a liquid flow path via a T-junction (Fig. 2a), and the gas–liquid mixture flowed down the serpentine channel in slug (or annular) flow – depending on the gas-to-liquid ratio – before reaching the catalytic bed. At the end of the microchannel, retention posts were used to retain the catalyst.

The catalyst powder (Section 2.1) was pelletised, crushed, and sieved to obtain the required sieve fraction (63–75 μm). The particle size was measured with a microscope (VHX-600 Digital Microscope, Keyence) and was found to be 65 ± 14 μm. Catalyst granules were loaded into the microreactor by applying a vacuum to the outlet port, with 1 mm and 3 mm length of glass beads (particle size of 60–70 μm) preceding and succeeding the catalytic bed respectively (Fig. 2b). The catalyst amount ranged between 1 and 4 mg (depending on the liquid flow rate) to keep the contact time constant in all experiments. Liquid alcohol (benzyl alcohol 99.98%, Sigma-Aldrich) was delivered into the reactor by a syringe pump (Ph.D. Ultra, Harvard Apparatus) and oxygen (N5.5 grade, BOC) delivered and regulated by a mass flow controller (Brooks 5850TR, Brooks Instrument). The effluent from the reactor flowed into a 2 ml glass vial located in a cold trap (iced beaker), where gas and liquid were separated and the liquid product was collected for analysis. The reactor temperature was controlled at 120 °C using a heating and temperature control unit (Watlow CAL 9900, Watlow Ltd.) consisting of a ceramic packing containing thermocouples and heating cartridges. The pressure was regulated to 1 barg in all experiments using a backpressure regulator (SS BP Regulator, Swagelok).

Start-up procedures consisted of oxygen flow at reaction temperature for one hour, followed by introduction of the liquid. Sampling was carried out every 30 min until stable operation was reached. Two to three samples were taken once steady state was reached and an average was taken of the duplicate or triplicate samples. When studying the effect of flow regimes, the gas flow rate was increased sequentially from low-to-high to avoid the interference of any hysteresis effects. Standard reaction runs (L=3 μl/min; G=0.6 Nml/min; 4 mg catalyst; 120 °C; 1 barg) were

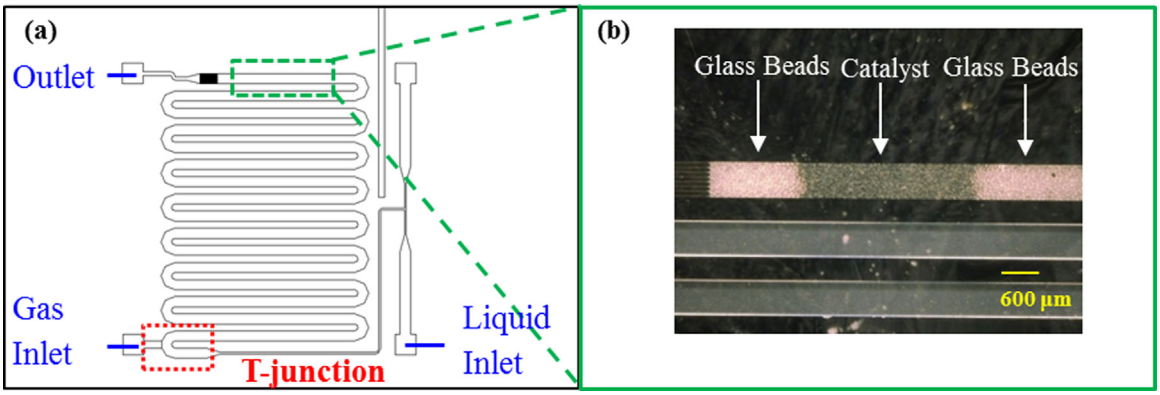

Fig. 2. (a) Schematic of the microchannel reactor with the gas–liquid introduction ports and (b) microchannel reactor packed with catalyst and glass beads.

carried out every 5–6 data points to ensure that the catalyst activity and selectivity did not change with time on stream. Quantitative analysis of the liquid samples was carried out using a gas chromatograph (Agilent 6890) with an FID detector, a HP-INNOWax (19091-133) capillary column and an auto-liquid-sampler. For GC analysis, 10 μl of the collected sample was diluted with 0.5 ml of 3% (v/v) butanol in o-xylene as an external standard.

Blank experiments were carried out where a typical reaction mixture (containing benzyl alcohol, benzaldehyde and toluene at a composition representative of 70% conversion) was fed into an empty microreactor at reaction conditions (120 °C and 1 barg) and the sample analysed at the exit. Results showed the mixture composition was unchanged, indicating the absence of a homogeneous reaction and confirming no loss of components into the gas phase.

Operating conditions were selected such that variables (other than the gas and liquid flow rates) were controlled and kept constant, yielding an experiment that probes solely the effect of hydrodynamics on reaction performance. The contact time, defined as the mass of catalyst over the mass flow rate of alcohol, was kept constant at 76 $g_{cat}\ g_{alc}^{-1}$ s in the micro-packed bed reactor (MPBR). This was achieved by altering the mass of catalyst as the liquid flow rate was changed (i.e. the bed was re-packed for different liquid flow rates). The bed density was ~0.75 g/cm^3 and did not vary significantly with re-packing, as the channel depth was maintained at ~300 μm (± 10 μm) and the particles were from the same batch of sieved catalyst particles (~65 ± 14 μm). Standard reaction runs were performed once the reactor was repacked to ensure repeatability.

2.3. Batch glass stirred reactor (GSR)

Batch experiments were carried out in a Radleys carousel reactor using a 50 ml glass stirred reactor (GSR) agitated using a magnetic bar. In a typical reaction, the requisite amounts of catalyst (20 mg) and substrate (2 g) were charged at room temperature into the reactor, which was then purged with the required gas (O_2) three times before the reactor was sealed using a Teflon screw threaded cap. The GSR was always connected to the gas-line to ensure the consumed gas was replenished. The pressure was monitored using the pressure gauge fitted at the inlet line. The reactor with the reaction mixture was loaded into a preheated heating block, which was maintained at the reaction temperature of 120 °C and pressure of 1 barg. The reaction started by commencing stirring inside the reactor at 1000 rpm. After 1 h reaction time, the stirring was stopped and the reactor was immediately cooled in an ice bath. After cooling for 10 min, the reactor was opened slowly and the contents were centrifuged. An aliquot of the clear supernatant reaction mixture (0.5 ml) was then diluted with mesitylene (external standard, 0.5 ml) for GC analysis. It was also verified that no reaction occurred in the absence of the catalyst or in the presence of the catalyst support alone. This experimental method is identical to our standard reaction protocols for solvent-free benzyl alcohol oxidation reported elsewhere (Sankar et al., 2012).

Comparisons are made in the Results section to batch reactor experiments conducted at a contact time of 38 $g_{cat}\ g_{alc}^{-1}$ s, where contact time in the glass stirred reactor is defined as the mass of catalyst multiplied by the reaction time over the initial mass of alcohol. Preliminary studies with the micropacked bed reactor showed that selectivity was not affected for contact time > 5 $g_{cat}\ g_{alc}^{-1}$ s (Fig. 3) and therefore the differences in the contact times between the two reactors can be ignored when making comparisons of benzaldehyde selectivity.

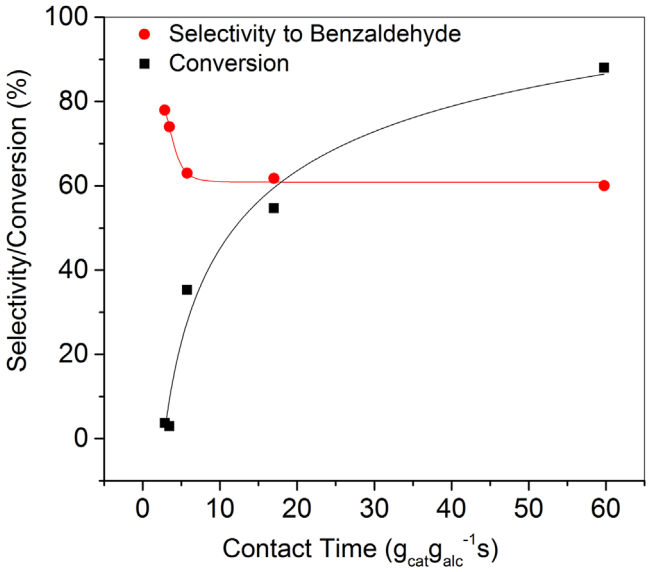

Fig. 3. The effect of contact time on benzyl alcohol conversion and selectivity to benzaldehyde. Liquid flow rate: 5 μl/min; *G:L* Ratio: 200; Temperature: 120 °C; Pressure: 1 barg.

2.4. Flow mapping

The flow mapping experiments were performed with benzyl alcohol as the liquid feed, oxygen as the gas feed and typical reaction temperature (120 °C) and pressure (1 barg). Superficial velocities were calculated based on the above conditions. The flow maps were generated with catalyst particles of 65 ± 14 μm and the typical catalyst bed length was 3.2 mm.

Flow observation was carried out via visualisation of the contacting patterns using a microscope (VHX-600 Digital Microscope, Keyence). To aid visualisation of the liquid, benzyl alcohol soluble red dye (Sepisol Fast Red, Bima 83) was dissolved in the flow medium. The dye tends to colour pink-yellow when the thickness of the liquid layer is large and red when the liquid layer is thin. The pressure drop during flow mapping was < 0.35 bar.

Flow mapping experiments were conducted by altering the gas or liquid flow rate until a transition was observed. Subsequently, it was probed further by smaller modifications to the gas and liquid flow until the exact transition point was determined. Spot-checks were carried out where the same point was repeated (once the bed was subjected to a different flow history) to ensure no significant hysteresis effects.

3. Results and discussion

3.1. Batch reactor performance

Reaction performance was first determined using a batch glass stirred reactor. The reaction products were predominantly benzaldehyde and toluene, with traces of benzoic acid and benzyl benzoate. Conversion in the glass stirred batch reactor at 1 h reaction time was 75.6%, and selectivity to benzaldehyde and toluene were 73.9% and 23.6% respectively.

3.2. Hydrodynamics in the micro-packed bed reactor

3.2.1. Flow pattern dependence on gas/liquid flow rates

Five main types of flow regimes were identified in the micropacked reactor (Figs. 4 and 5): liquid-dominated slug, segregated,

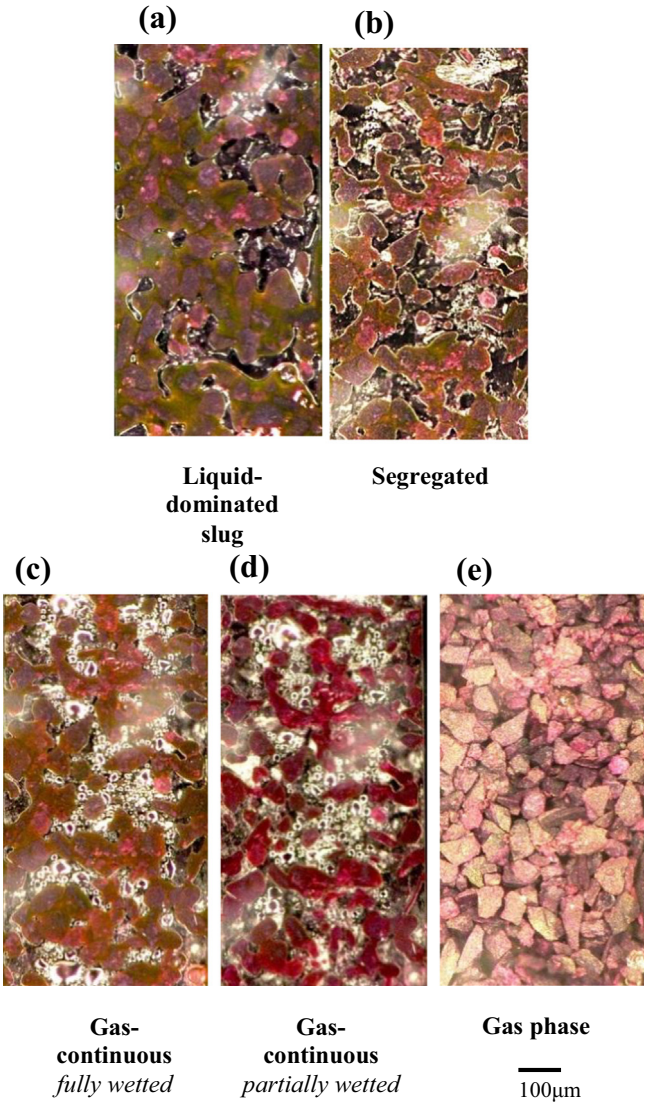

Fig. 4. Microscope images of the micro-packed bed reactor showing the flow regimes corresponding to Fig. 5. (a) Liquid-dominated slug (b) segregated (c) gas-continuous (fully wetted) (d) gas-continuous (partially wetted) and (e) gas phase.

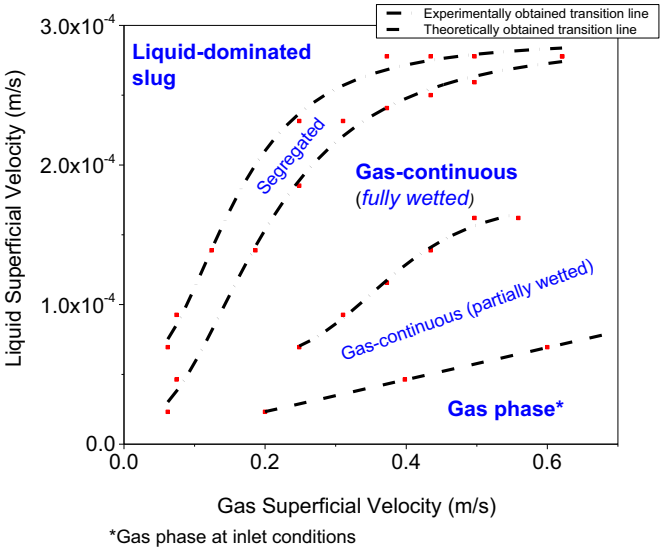

Fig. 5. Flow regimes observed in the micro-packed bed reactor for benzyl alcohol/oxygen flow system under representative reaction conditions (120 °C, 1 barg). Experimental data points utilised to obtain the curves are marked with red symbols. (For interpretation of the references to colour in this figure legend, the reader is referred to the web version of this article.)

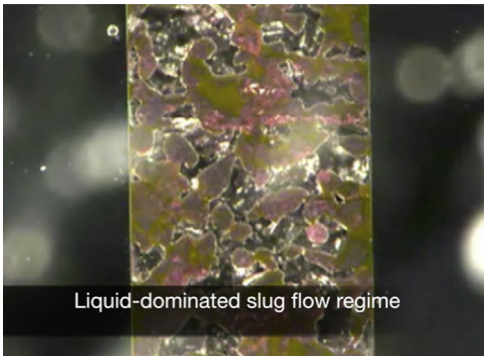

Video 1. Optical microscope observation of the hydrodynamics during liquid-dominated flow regime, u_L=9.3×10^{-4} m/s, u_G=0.31 m/s. Supplementary material related to this article can be found online at http://dx.doi.org/10.1016/j.ces.2016.03.018.

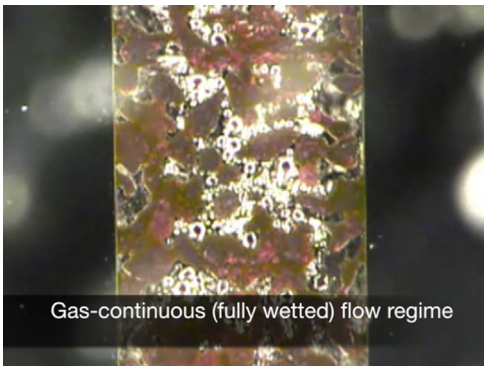

Video 2. Optical microscope observation of the hydrodynamics during gas-continuous (fully wetted) flow regime, u_L=6.9×10^{-5} m/s, u_G=0.24 m/s.Supplementary material related to this article can be found online at http://dx.doi.org/10.1016/j.ces.2016.03.018.

gas-continuous (fully wetted), gas-continuous (partially wetted), and a gas phase flow regime. The flow regime transitions occurred as a result of changes in the gas (G) and liquid (L) flow rates. High gas in conjunction with low liquid flow rates favoured gas-continuous flow, while low gas and high liquid flow rates favoured liquid-dominated slug flow.

Liquid-dominated slug flow exhibited regions of gas and liquid, where liquid occupied the majority of the bed and covered the particle interstitial voids, while the gas formed large elongated slugs, leaving the gas–liquid surface to reside at the interface of a few gas voids (Fig. 4a). Under this flow regime, slug flow was observed upstream the packed bed, causing liquid-rich waves or "pulses" to traverse the bed length at regular time intervals (see Video 1 in Supplementary information). The term slug also identifies the behaviour inside the packed bed, as at some points in time the fluid extends throughout the channel cross-sectional area. This is a form of induced pulsing, usually achieved in conventional reactors by on-off liquid or gas flow modulation. Natural pulse flow (which forms as a result of global convective instability in the packed bed region) is usually associated with better mass transfer than trickle flow. Similar to natural pulsing, the motivation for induced pulsing (via on-off flow modulation) is to reduce the resistance to the gas transfer caused by the presence of the liquid film.

With an increase in gas and decrease in liquid flow rate, a transitional flow regime existed – segregated flow – where gas and liquid had a similar and constant share of the bed without

significantly perturbing each other (Fig. 4b). Wavy-annular flow in the empty channel upstream of the packed bed was usually observed with this type of flow and the resulting segregated flow pattern in the packed bed was often dynamic in nature – caused by liquid waves propagating from the empty channel upstream.

The transition to gas-continuous flow takes place with a further increase in gas/decrease in liquid flow rate. This flow regime consisted of a continuous gas phase whilst the liquid formed a more uniformly distributed thin film surrounding the catalyst particles (Fig. 4c) – a flow pattern which has been associated with trickle flow in conventional trickle bed reactors (see Video 2 in Supplementary information). The term "trickle" is not used in this work due to the dominance of capillary forces.

At elevated gas-to-liquid ratios, partial drying of the catalyst particles took place, where the liquid travelled along the packed bed in the form of "rivulets" rather than in the form of a film, leaving some parts of the particles exposed to the gas (Fig. 4d). Finally, with a further increase in gas velocity the flow transitioned into a gas phase regime (Fig. 4e). In order to capture the onset of this transition accurately, this transition line was calculated based on vapour–liquid equilibria, using the vapour pressure of benzyl alcohol and the ideal gas law to determine the gas flow rate at which all benzyl alcohol would be in the gas phase for each liquid flow rate. It is important to note that this transition relates to the inlet conditions prior to the packed bed. The situation is more complex inside the packed bed where capillary condensation and evaporation would be taking place. This may result in pellets that are non-wetted on the external surface but that are partially filled with liquid due to capillary condensation.

3.2.2. Flow pattern and dynamics: dependence on upstream flow conditions

The dynamic state inside the catalytic bed was highly dependent on the flow pattern establishment upstream, which in itself was dependent on the gas–liquid introduction method. The microreactor used in this work introduces gas into a liquid flow path via a T-junction, producing either slug or annular flow, depending on the gas-to-liquid (*G*:*L*) flow rate ratio. At low *G*:*L*, the flow pattern preceding the bed was slug flow, which manifested in dynamic behaviour in the catalytic bed, consisting of periodic wetting and drying of the particles (high interaction). The liquid-dominated slug flow regime is analogous to induced pulsing in conventional reactors, where the liquid is modulated on/off to promote the gas–solid mass transfer in between liquid bursts. Intermediate *G*:*L* resulted in wavy-annular flow upstream causing slight movement of the gas–liquid boundary layer as the wave propagated through the packed bed. High *G*:*L* resulted in annular flow upstream and consequently stable flow conditions in the packed bed, with the gas and liquid not significantly engaging with each other (low interaction).

The segregated and gas continuous flow regimes are analogous to trickle flow in conventional trickle bed reactors. The segregated flow regime is characterised by a thick liquid film segregating the gas domains, while the gas-continuous has a thin film covering the catalyst particles, which changes to thin rivulets at very high (low) gas (liquid) flow rates, leading to partial wetting. Using the classification in Table 1, it is possible to predict the flow regime in the catalytic bed by observing the flow pattern in the empty channel preceding it.

3.2.3. Comparison with macro-scale flow maps

The flow regime observed in the microchannel reactor is a result of the interplay of gravitational, surface tension, inertial and viscous forces, giving rise to varying levels of flow instabilities and fluid phase distributions. The relative importance of these factors differs in microchannels compared to conventional scale reactors, due to higher capillary/surface tension forces and negligible gravitational contribution. The Bond number, *Bo*, quantifies the relative importance of gravity with respect to surface tension forces and was calculated to be 2.12×10^{-3} using the particle diameter as the characteristic length, indicating the dominance of interfacial forces. This value is 2–3 orders of magnitude smaller as compared to conventional reactors where the *Bo* number usually lies within 0.1–10 (de Santos et al., 1991). Eqs. (1)–(3) refer to the relevant dimensionless numbers governing the hydrodynamics in a trickle bed reactor and Table 2 presents a comparison of these dimensionless numbers between reactors of different scales.

$$Re_L = \frac{\rho_L u_L d_p}{\mu_L} \qquad \frac{inertial\ force}{viscous\ force} \tag{1}$$

$$Ca_L = \frac{\mu_L u_L}{\sigma} \qquad \frac{viscous\ force}{capillary\ force} \tag{2}$$

$$Bo = \frac{(\rho_L - \rho_G) g d_p^{\,2}}{\sigma} \qquad \frac{gravitational\ force}{capillary\ force} \tag{3}$$

The values in Table 2 demonstrate the dominance of the viscous and capillary forces in relation to inertial and gravitational forces in the MPBR. The very low Reynolds (0.01–0.03) number in the MPBR translates to a liquid flow that is laminar in nature and the low Bond (2.12×10^{-3}) and Capillary (1.8×10^{-6}–7.4×10^{-6}) numbers indicate the relative strength of the capillary forces in comparison to conventional laboratory and industrial trickle bed reactors. This is in agreement with observations by Alsolami et al. (2013), who envisaged that small particles lead to high capillary forces and thus poor radial dispersion of the liquid phase. In their particular case, product inhibition – caused by poor radial mass transport from the liquid to the gas phase – was evident in their microflow reactor.

Fig. 6 shows the flow regime transitions observed in the current work (transition from liquid-dominated slug to segregated) compared to that of the Charpentier and Favier flow map (transition from pulse to trickle) for a conventional trickle bed, plotted on the Baker coordinates (Charpentier and Favier, 1975). The transition from high interaction to low interaction regime appears to take place at *L*:*G* ratios one order of magnitude smaller in the micro-packed bed reactor (in the current work), a difference that is not surprising given the previous analysis of forces.

The existing literature on flow regimes identified in micro-packed bed reactors differs in the reactor design, the flow regime

Table 1
Characterisation of flow regimes observed in the micro-packed bed reactor and their relationship with the flow pattern upstream the packed bed section.

G:*L* ratio	Flow regime upstream of packed bed	Flow regime in packed bed	Dynamic/steady-state	High interaction/low interaction	Analogous to – in the macroscale
High	Annular	Gas-continuous and gas phase	Steady-state	Low interaction	Trickle (thin film and rivulet flow)
Intermediate	Wavy-annular	Segregated	Dynamic	Low interaction	Trickle (thick liquid film)
Low	Slug	Liquid-dominated slug	Dynamic	High interaction	Induced pulsing

Table 2
Values of key dimensionless parameters in various reactor scales.

	Micro-packed bed reactor	Typical laboratory scale reactor[a]	Industrial trickle bed reactor[b]
Reactor diameter (m)	0.0004	0.1	1
Particle diameter (m)	6.50×10^{-5}	3.00×10^{-3}	3.00×10^{-3}
Re_L	0.01–0.03	1.5–40	31.2
Ca_L	1.8×10^{-6}–7.4×10^{-6}	7.3×10^{-6}–2.2×10^{-4}	1.86×10^{-4}
Bo	2.12×10^{-3}	1.16	4.66

[a] Dimensionless numbers calculated from Charpentier and Favier's study for air/water (Charpentier and Favier, 1975).
[b] Industrial trickle bed reactor data obtained from Alsolami et al. (2013).

classification, and their agreement with the conventional Charpentier and Favier flow map. Whilst some authors reverted to the conventional terminology of "trickle" and "pulse" commonly used in conventional reactors (Losey et al., 2001; Inoue et al., 2015), others have designated new classifications for the observed flow regimes (Faridkhou and Larachi, 2012). It is important to note the differences between the designs of microchannel reactors and that of conventional packed bed reactors, which has direct implications on the flow pattern development. In a microchannel reactor, the gas and liquid are commonly introduced upstream of the packed bed via a T-junction configuration. The presence of void spaces between the inlet and the packed bed region gives rise to the formation of a slug flow pattern, with alternating gas and liquid slugs traversing the packed bed. Faridkhou and Larachi (2012) have identified this as an instability and thus introduced the liquid directly into the packed bed section to preclude the formation of liquid slugs and to imitate typical operation in conventional reactors. The transition from high interaction to low interaction was found to take place at L:G ratios three orders of magnitude smaller than Charpentier's, indicating that the differences in the flow regime transition are due to differences in the dominant forces within the packed bed, in addition to the gas–liquid introduction method. Conversely, Losey et al. (2001) – who had a similar type of inlet design to the current study – found a transition line between pulse and trickle which was 0-1 orders of magnitude lower than the Charpentier flow map. The similarity in microreactor designs between this study and that of Losey et al. (in terms of gas–liquid introduction method that results in a void upstream the packed bed) may have led to the similarity in the flow regime transition. Contrary to all other microreactor studies, Inoue et al. (2015) had a flow map which agreed very well with Charpentier's and attributed this to the gas flow stabilisation by a pressure drop mechanism (applying a high pressure drop on the gas side upstream the microreactor). The difference of the flow transition (between bubbly slug and annular flow regimes) obtained by Krishnamurthy and Peles (2007) may be related to the nature of the bed, which was a forest of isolated microfabricated posts. In addition, glass beads were used by Faridkhou and Larachi (2012) whereas porous catalyst particles were used in the remaining studies, which may have contributed to the observed differences. Therefore, comparisons between hydrodynamic studies in micro-packed beds are difficult to make given the differences in geometries of the gas/liquid inlet, as well as the type of packing used, which all play a role in the type of flow pattern that forms. Furthermore, at these reduced dimensions, effects of wall roughness, wettability and flow confinement become important (Shao et al., 2009).

In contrast to macro-scale reactors, natural pulsing was not observed. The origin of pulsing detected at low G:L ratios was induced by the slug flow upstream of the packed bed section. This lack of natural pulsing behaviour has been reported in previous hydrodynamic studies in micro-packed bed reactors (van Herk et al., 2005) and is not surprising for a Reynolds number of the order of 1, where inertia-induced pulsing is unlikely. The usual mode of entry for gas and liquid phases in a conventional packed bed reactor is at the top of the column, where a liquid distributor is used to irrigate the bed evenly with the liquid phase. The forced

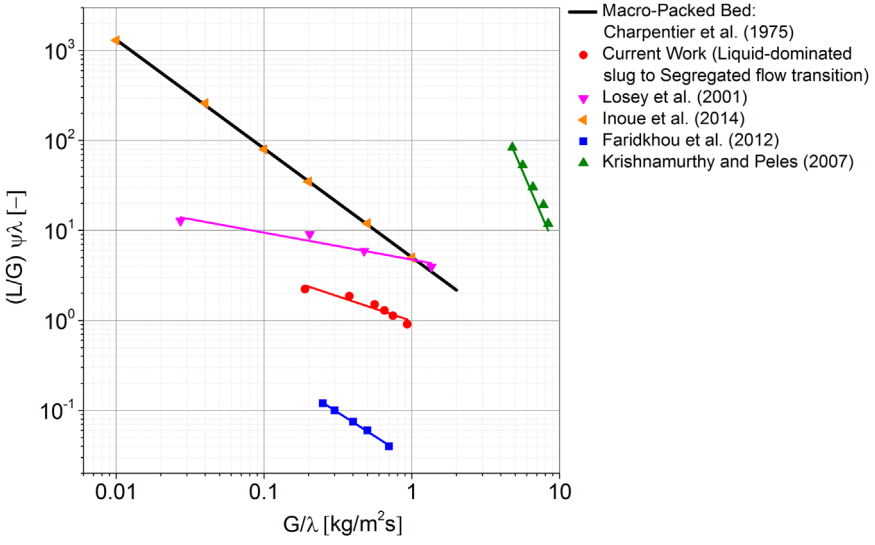

Fig. 6. Flow map comparison of a conventional trickle bed reactor: Charpentier and Favier (1975) and micro-packed reactors: Faridkhou and Larachi (2012), Losey et al. (2001), Krishnamurthy and Peles (2007) and Inoue et al. (2015) using the Baker Chart Parameters $\lambda = \left[\left(\frac{\rho_G}{\rho_A}\right)\left(\frac{\rho_L}{\rho_W}\right)\right]^{0.5}$ and $\psi = \frac{\sigma_W}{\sigma}\left[\left(\frac{\mu_L}{\mu_W}\right)\left(\frac{\rho_W}{\rho_L}\right)^2\right]^{1/3}$.

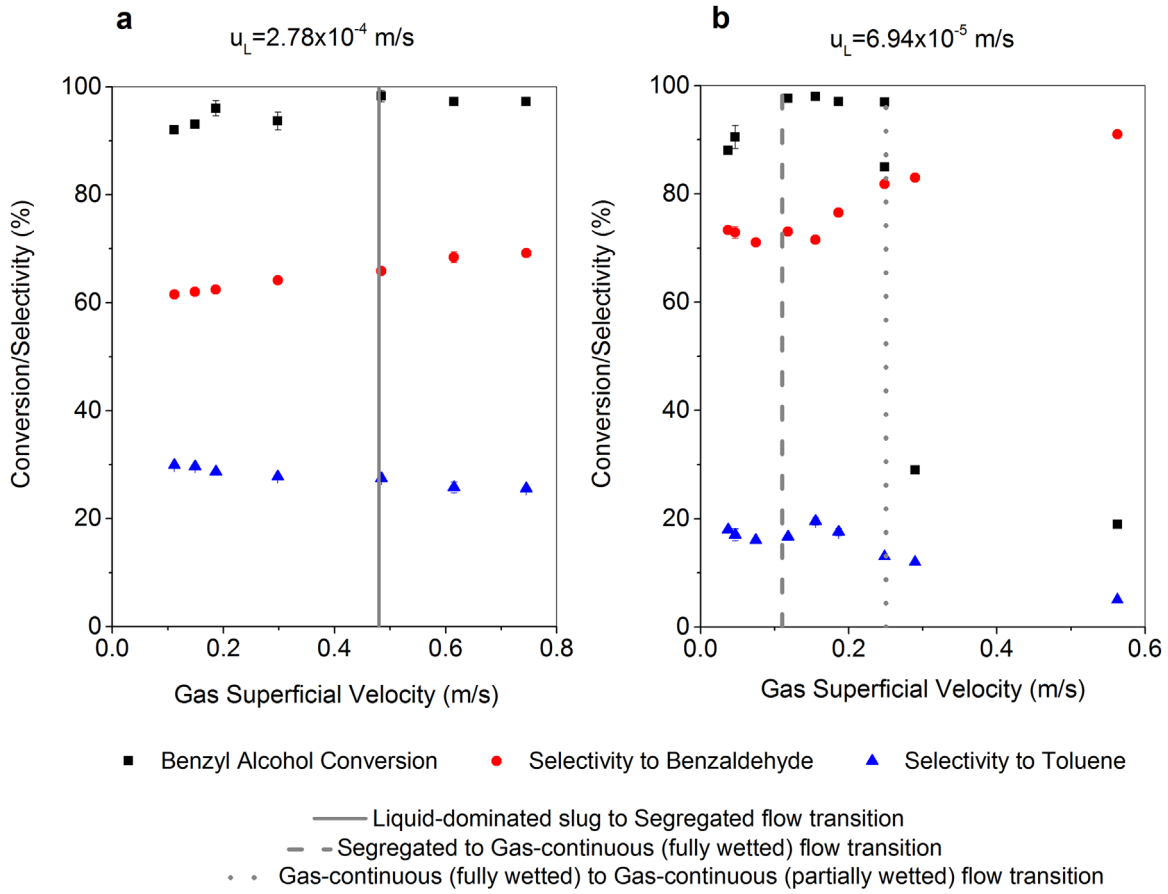

Fig. 7. Conversion of benzyl alcohol and selectivity to benzaldehyde and toluene at various flow regimes obtained by increasing gas flow rate. (a) Liquid-dominated slug transitioning into segregated flow regime at liquid flow rate 3 μl/min (b) segregated transitioning into gas-continuous (fully wetted) and subsequently to gas-continuous (partially wetted) flow regime at liquid flow rate 0.75 μl/min.

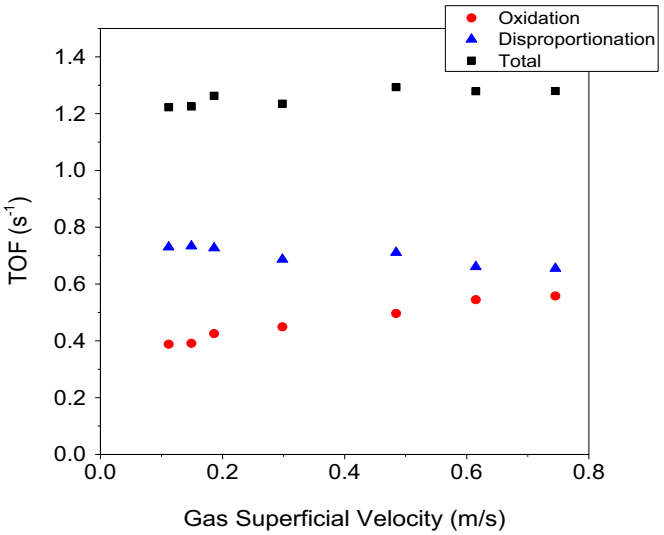

Fig. 8. Dependence of average TOF_O, TOF_D and TOF_T on gas superficial velocity corresponding to the data in Fig. 7a.

pulsation is therefore usually achieved in conventional reactors by forced time varying liquid (Boelhouwer et al., 2002) or gas flow rates (Xiao et al., 2001).

The spray regime commonly observed in conventional packed bed reactors was not observed in the micro-packed bed, and this is attributed to the dense packing and small interstitial voids, precluding the existence of liquid droplets between the catalyst particles. Instead, a predominantly gas phase regime exists in the micro-packed bed reactor.

3.3. Impact of hydrodynamics on reaction performance

With characterisation of the hydrodynamic conditions in the micro-packed bed reactor, we are now in a position to assess their influence on the catalytic benzyl alcohol oxidation reaction performance. We are interested in a higher benzaldehyde yield and will therefore be looking at the conversion and selectivity as performance indicators.

3.3.1. Liquid-dominated slug and segregated flow

Fig. 7a shows the change in reaction performance as the hydrodynamics change from liquid-dominated slug flow to segregated flow with increase in gas flow rate. The increase in conversion and selectivity with increasing gas flow rate is attributed to an enhancement in the gas–liquid mass transfer, which comes as a result of the increase in the gas–liquid interfacial area and decrease in film thickness. A high availability of oxygen at the catalyst active sites favours the oxidation reaction pathway, producing more benzaldehyde. Fig. 8 shows the dependence of TOF_O, TOF_D and TOF_T on gas superficial velocity. The TOF_D decreases and the TOF_O increases as the gas superficial velocity is increased, indicating the enhancement of the desired oxidation pathway which leads to increase of benzaldehyde selectivity. The overall turnover frequency, TOF_T, increases with gas superficial velocity, which conforms with the increase in conversion observed in Fig. 7.

A high dependence of mass transfer on gas flow rate under pulse flow in a conventional trickle bed reactor (analogous to the liquid-dominated slug) has been demonstrated in the past. The influence that gas flow rate has on the gas–liquid mass transfer rate has been attributed to an increase in the interaction between the gas and liquid phases as well as the spreading of liquid (Ranade et al., 2011; Hirose et al., 1974). The underlying phenomena governing this relationship between gas flow rate and increase in the gas transfer to the solid, is a decrease in the characteristic length (film thickness) across which the gas has to travel – this results in a higher gas–liquid mass transfer coefficient, k_{GL}, according to the film theory of diffusion (k_{GL} is the mass transfer coefficient corresponding to the liquid film of the gas–liquid interface. As the gas phase is pure oxygen, it is plausible to assume no mass transfer resistances exist at the gas film). The observed increase in gas–liquid interfacial area, a_{GL}, also has an effect on the overall rate of mass transfer across the gas–liquid interface (Doraiswamy, 2001).

Evidence of increase in mass transfer with gas flow rate due to an enhancement in the liquid–solid mass transfer, k_{LS}, is not widespread (Ranade et al., 2011) although an improvement in the liquid–solid mass transfer is possible with higher gas flow rate due to the larger linear velocities, as well as improvements in wetting and contacting between the packing and the flowing liquid (Hirose et al., 1976; Goto and Smith, 1975). For smaller packing (<0.5 mm), liquid–solid mass transfer rates were found to be slightly higher in liquid beds without gas flow, and this was attributed to the fact that in a packed bed with smaller particles, the entire external area is not effective for mass transfer and this effect predominates over the effect of an increase in velocity (Goto and Smith, 1975).

3.3.2. *Gas-continuous (fully wetted and partially wetted) flow*

Fig. 7b shows the reaction performance in the gas-continuous (fully wetted) and gas-continuous (partially wetted) flow regimes. Initially, no significant change in selectivity occurs and conversion plateaus with increasing gas flow rate. This indicates that the increase in gas flow rate – whilst operating in the gas-continuous flow regime – does not affect mass transfer significantly, as the liquid film is sufficiently sheared and any further increase in gas flow has only a small additional benefit. Under partial wetting, the selectivity to benzaldehyde continues to increase and reaches values $>90\%$, however, a dramatic decline in the conversion is observed (Fig. 7b). The packed bed reactor begins to outperform the batch reactor (in terms of selectivity) under this partially wetted state, where there is the added benefit of gas–solid mass transfer at exceptionally high gas-to-liquid ratios. Selectivity to benzaldehyde reaches 93%, but this comes at the cost of approx. 80% reduction in conversion. At a gas-to-liquid flow rate ratio of 8000 ($u_G=0.55$ m/s in Fig. 7b) approximately 90% of the benzyl alcohol at the reactor inlet evaporates to the gas phase. At this point, there is direct contact between the catalyst surface and the oxygen on the dry surface of the catalyst particle, already wetted internally due to capillary forces, resulting in an increase in the benzaldehyde selectivity to 93%.

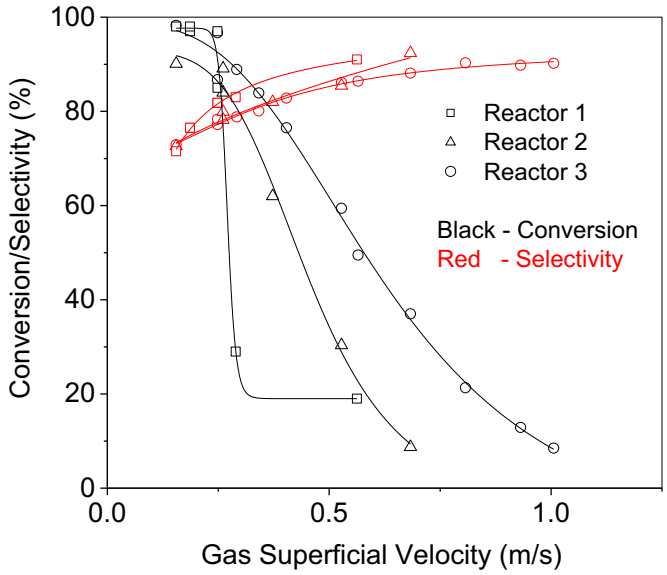

Fig. 9. Repeatability in the gas-continuous (partially wetted) flow regime using three different reactors, each re-packed with a new bed of catalyst. Liquid superficial velocity: 6.94×10^{-5} m/s, Catalyst mass: 1 mg.

The drop in conversion is postulated to be due to poor utilisation of the catalyst particles caused by incomplete wetting (despite some liquid remaining due to capillary forces, maintaining some reactant conversion). In the liquid-dominated slug flow regime, the combination of a liquid film that is incompletely saturated with oxygen and a rapid reaction, leads to a rate that is limited by the external supply rate of the gaseous reactant. In such a situation, the more effective supply route for the gaseous reactant is through the non-wetted surface, where there is no resistance to its mass transfer. However, at sufficiently high gas and low liquid flow rates (partially wetted state), the fraction of the surface wetted by the liquid is sufficiently low that the mass transfer of the liquid reactant becomes limiting. Fig. 7a and b, indicate that a maximum in the conversion exists at an intermediate level of wetting (the gas-continuous fully wetted flow regime). This maximum results from a competition between two different limiting regimes: at sufficiently low liquid coverage, the reaction is limited by the supply of the liquid reactant, whereas at higher liquid coverage it is gas-reactant-limited. Such behaviour has been observed previously by Funk et al. (1991) in the hydrogenation of α-methylstyrene, as well as Hodoshima et al. (2003) in the dehydrogenation of decalin.

The abruptness of the drop may be due to a critical phenomenon where a percolation threshold has been reached, and the links between the rivulets flowing along the packed bed are disconnected due to the increase in gas flow rate. This drop in conversion was difficult to reproduce quantitatively in repeated experiments (Fig. 9). This was possibly because the liquid may be distributed differently within the packed bed each time a new reactor was loaded. Some evidence of deactivation was also observed in this partially wetted state, the degree of which was dependent on the gas flow rate and duration of operation, and was (in some cases) irreversible upon re-wetting of the catalytic bed. It is possible to increase the conversion by packing the microreactor with more catalyst and effectively increasing the contact time. Experiments were carried out with seven times more catalyst (7 mg), which resulted in an increase in conversion from 20% to 81%, while the selectivity was maintained at 92%. Such performance is superior to the batch glass stirred reactor in terms of both conversion and selectivity.

With regards to existing studies in the literature investigating hydrodynamic effects on reaction, studies on periodic flow operation have shown that this type of operation is beneficial in gas-limiting reactions, where the direct access of the gaseous reactant to the solid surface improves the gas-to-catalyst mass transfer (Ranade et al., 2011). The reactor type can also influence the mass transfer, where structured packings (in the form of catalytically active membranes) have also been used as a solution to reactions with liquid phase transport resistance, by acting as a means of segregating the gas and liquid, thus providing direct access of the gas to the catalyst surface (Yang and Cussler, 1987).

Studies comparing mass transfer coefficients in gas–liquid

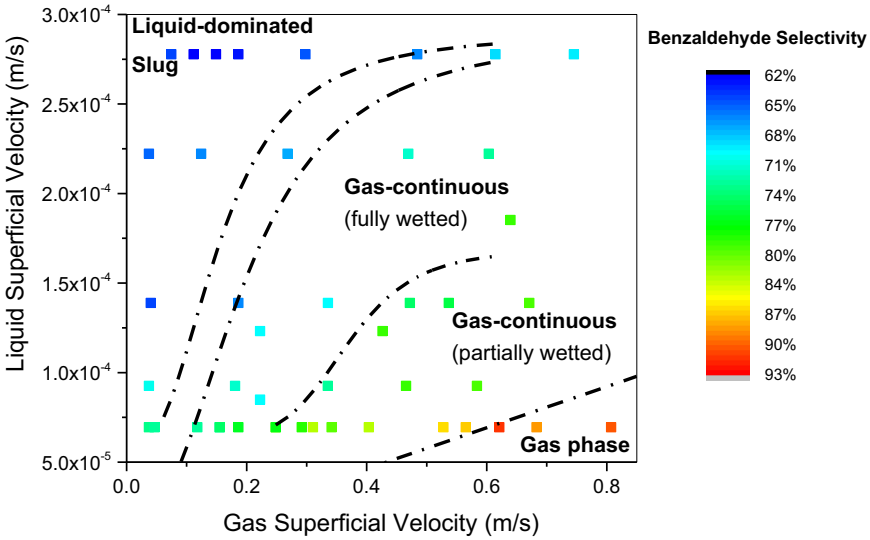

Fig. 10. Benzaldehyde selectivity colour-mapped dot plot superimposed on the flow regime map.

reactions between trickle bed reactors (TBR), hollow fibre membrane reactors (HFR) and stirred tank reactors (STR) have shown that the ranking of reactors, in terms of mass transfer, was HFR > TBR > STR. While the enhancement in the TBR is attributed to minimisation of the liquid resistance to mass transfer due to the thinner liquid film, the HFR outperformed both other reactors due to a large surface area-to-volume ratio and the absence of a liquid film (barrier to gas transfer) (Orgill et al., 2013). Operating a micro-packed bed reactor (which has a large surface-area-to-volume ratio) in the gas-continuous flow regime (where there is minimal liquid phase resistance) therefore brings together the advantages of both the TBR and the HFR.

3.4. Relating reaction performance to the flow map

Further experiments were conducted to validate the proposed association between flow regime and reaction performance, as well as extend the operating window into the gas phase regime. A total of 42 experiments were used to generate a colour mapped dot plot of conversion and selectivity to benzaldehyde superimposed on the flow regime map, shown in Figs. 10 and 11.

There is a clear relationship between selectivity and flow pattern. Improved distribution of liquid, a thinner liquid film and a larger gas–liquid interfacial area are obtained with increasing gas velocity, enhancing mass transfer and therefore the transfer of oxygen to the catalyst active sites, promoting the oxidation reaction that produces benzaldehyde exclusively (Fig. 10). With partial drying of the catalyst particles, direct gas–solid mass transfer is promoted, which further enhances the overall oxidation reaction rate, increasing benzaldehyde selectivity. The colour mapped dot plot for conversion (Fig. 11) shows a slightly different pattern to that of the selectivity graph, where the aforementioned drop in conversion in the partially wetted flow and gas phase regimes is clear. It is worth noting that the observed variability in conversion at high gas flow rate (Fig. 9) has an impact only for $u_G = 3420u_L$, where partial wetting begins to severely affect the conversion, however, it does not have an effect on the overall trends observed. Figs. 10 and 11 were plotted using results from all three reactors in Fig. 9.

3.5. Response surface model

A response surface methodology (RSM) (Box and Draper, 1987) was applied for two main purposes: i) investigating the

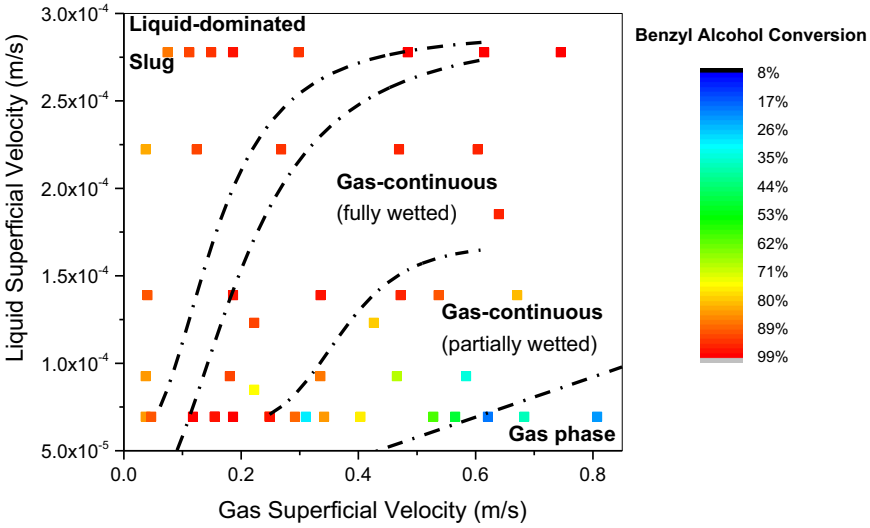

Fig. 11. Benzyl alcohol conversion colour-mapped dot plot superimposed on the flow regime map.

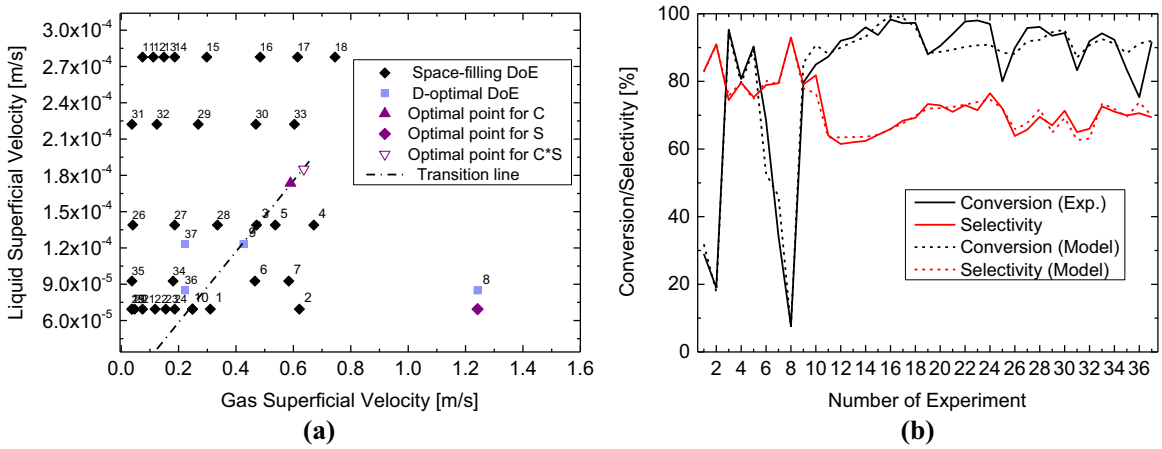

Fig. 12. Response surface methodology results: (a) allocation of experiments in the design space (black points represent experiments carried out according to the space-filling DoE, blue points represent experiments proposed by a D-optimal DoE, purple points represent optimal points for C, S and yield (product C·S) as predicted by the model); and (b) conversion and selectivity: experimental values (solid line) and values predicted by the model (broken line). (For interpretation of the references to colour in this figure legend, the reader is referred to the web version of this article.)

relationship between conversion/selectivity and gas and liquid superficial velocities quantitatively within the observed hydrodynamic regions; ii) design of experiment (DoE) purposes (Montgomery, 2005) in order to find the combinations of experimental factors achieving the minimal variability in the response. After a preliminary model discrimination step, the best model structure found to provide a satisfactory representation of both conversion and selectivity at the investigated experimental conditions was a quadratic model with quadratic interaction in the form:

$$Y = Y_0 + \sum_{i=1}^{N_F} a_i F_i + \sum_{i=1}^{N_F} \beta_i F_i^2 + \sum_{(i\neq j)=1}^{N_F} \gamma_i F_i F_j + \sum_{(i\neq j)=1}^{N_F} \delta_i (F_i F_j)^2 \qquad i = 1 \ldots N_F \tag{4}$$

In (4), Y is the observed (measured) response (benzyl alcohol conversion C or selectivity to benzaldehyde S), F_i represents the i-th experimental factor (here $N_F=2$, $F_1=u_L$, $F_2=u_G$) and Y_0, α_i, β_i, γ_i, δ_i are the model parameters to be estimated from experimental data. The allocation of experimental points in the design space is shown in Fig. 12a. A total of $N=37$ experiments were executed and used in order to investigate the behaviour of the system in the space of experimental conditions (u_G=0.04–1.24 m/s, u_L=7–27.7E−05 m/s), of which 33 were planned according to a space-filling DoE in the region u_G=0.04–0.77 m/s, u_L=7–27.7E−05 m/s (i.e. a design where experimental points were distributed along this experimental region), while 4 additional experiments were proposed by a D-optimal DoE. According to the D-optimal DoE, u_G and u_L were computed in order to minimise the uncertainty on model prediction (Box and Draper, 1987). In the design procedure, a linear regression of the experimentally obtained transition line points between the gas-continuous (fully wetted) and gas-continuous (partially wetted) hydrodynamic regions was carried out. The transition between the two regions was approximated by the following linear relationship between the design factors:

$$u_G = k^* u_L. \tag{5}$$

where $k=3420$. This expression is required to represent the sudden decrease in the conversion experimentally observed in the gas phase regime, since two distinct parametric sets for the model (4) have to be used in the proximity of the transition line (5) for describing the conversion above and below $u_G=3420u_L$ (gas-continuous/fully wetted flow transition).

Parameter estimation results obtained after fitting model (4) to the full set of experimental points are given in Table 3, while Fig. 12b shows the model performance in terms of conversion/selectivity representation. The model is able to represent the experimental data reliably, particularly with respect to the selectivity. In fact, for selectivity the mean absolute error is close to 2%, while the representation of conversion is more critical (mean absolute error close to 4). Response surface plots are shown in Fig. 13 for conversion and selectivity.

The RSM model is used for the evaluation of optimal experimental conditions (G, L) maximising conversion (C), selectivity (S) and yield ($C\cdot S$), by formulating and solving the following optimisation problem:

$$f^{MAX} = \max_{u_G, u_L} f(\boldsymbol{\theta}, u_G, u_L) \tag{6}$$

subject to the model Eq. (4) and to the following constraints in the investigated hydrodynamic region:

$$0 < u_G < 1.6 \text{ m/s} \tag{7}$$

$$0 < u_L < 3.7\text{E}-04 \text{ m/s} \tag{8}$$

In (6) f is the function being maximised (C, S, or $C\cdot S$), f^{MAX} is its

Table 3
Parameter estimation results obtained from data fitting above ($u_G \geq 3420u_L$) and below ($u_G < 3420u_L$) the transition line.

Response	Model parameters						
	Y_0	α_1	β_1	α_2	β_2	γ_1	δ_1
Conversion ($u_G \geq 3420u_L$)	8.41E−01	2.04E+03	3.88E+05	5.12E−03	1.08E−04	3.53E+01	2.43E+02
Selectivity ($u_G \geq 3420u_L$)	7.78E−01	−1.28E+02	2.52E+04	2.81E−02	4.70E−04	−7.72E+00	6.92E+01
Conversion ($u_G < 3420u_L$)	8.77E−01	−2.42E+00	−3.24E+03	1.61E−02	3.31E−03	7.09E+00	1.12E+02
Selectivity ($u_G < 3420u_L$)	7.78E−01	−1.28E+02	2.52E+04	2.82E−02	4.70E−04	−7.72E+00	6.92E+01

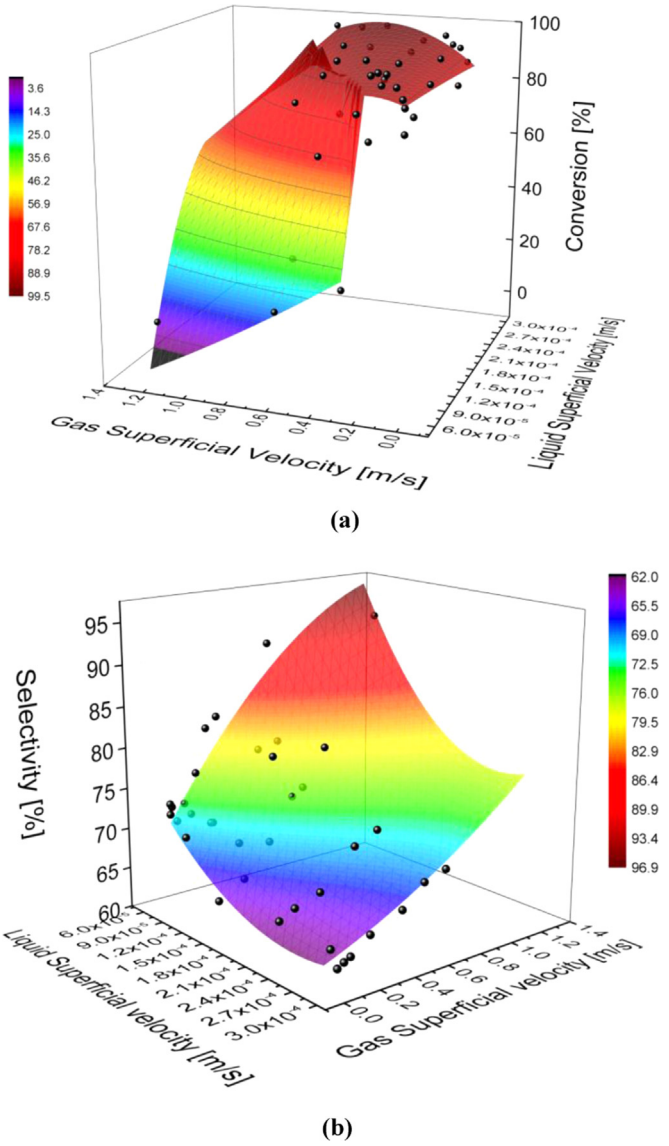

Fig. 13. Response surfaces: (a) conversion as a function of gas and liquid superficial velocities; (b) selectivity to benzaldehyde as a function of gas and liquid superficial velocities. In the graphs experimental points are indicated by black spheres.

maximum value and $\boldsymbol{\theta}$ is the set of parameters of the model (4). According to the formulation (6–8), the maximum conversion and selectivity are achieved, respectively, at

$$u_G = 0.59 \text{ m/s} \quad u_L = 1.7E-4 \text{ m/s} \rightarrow C = C^{MAX} = 99\%$$

$$u_G = 1.24 \text{ m/s} \quad u_L = 6.9\,E-5 \text{ m/s} \rightarrow S = S^{MAX} = 98\%$$

The optimal conditions maximising the yield are found to be at u_G=0.64 m/s and u_L=1.85E–4 m/s. At these conditions the model predicts $C=C^{MAX}$=99% and S=86%. Hence, relatively high gas superficial velocities (i.e. $u_G > 0.6$ m/s) should be used in conjunction with moderate liquid superficial velocities (i.e. u_L~1.4–1.85E−4 m/s) which is sufficient to ensure the full wetting of the catalyst bed in order to prevent a drop in conversion (see Fig. 13a). This prediction was checked by conducting an experiment at u_G=0.64 m/s (G=10.3 N ml/min) and u_L=1.85E−4 m/s (L=2 μl/min). The response surface model provides a 6% over-estimation on the benzyl alcohol conversion (C=99% against C=93% of the experiment) and selectivity to benzaldehyde (S=86% against S=80% of the experiment). As a result of error propagation, this over-estimation observed for C and S gives approximately a 10% over-estimation on optimal yield. The mismatch may be related to the uncertainty on characterising the measured responses when experiments are carried out around the transition region, despite the great reliability of the model at slightly lower liquid and gas superficial velocities. Nonetheless, these hydrodynamic conditions represent the best conditions to be used in the microreactor for obtaining a high yield, as the yield obtained surpasses that obtained in all experimental points presented previously.

4. Conclusions

The gas–liquid hydrodynamics in a packed bed microreactor during benzyl alcohol oxidation on Au–Pd/TiO_2 catalyst have been investigated. Results show hydrodynamics that are different from what is commonly observed in conventional multiphase packed bed reactors. Five flow regimes were identified, including liquid-dominated slug and gas-continuous flow. There are some similarities to the hydrodynamics in conventional packed bed reactors; for instance, the gas continuous flow regime observed in the microreactor is similar to trickle flow. However, there are also differences, such as the absence of natural pulsing (due to the lack of inertial forces) and spray (due to smaller size of voids) flow regimes. Thick liquid layers are observed at low gas and high liquid flow rates, resulting in low gas–liquid interfacial areas and consequently poor gas–liquid mass transfer.

The transition from liquid-dominated slug to gas-continuous flow appears to deviate from the conventional Charpentier and Favier flow map between pulse and trickle flow, with the transition happening at liquid-to-gas ratios one order of magnitude smaller. However, one has to be careful with this comparison as the flow pattern establishment upstream the packed bed in the microreactor plays a significant role in the hydrodynamics and flow regime in the packed bed section.

Operating the micro-packed reactor in the gas-continuous flow regime benefits from a sufficiently wetted catalyst with a gas continuous flow path, maximising the gas–liquid interfacial area and minimising the liquid film thickness, thus enhancing the external mass transfer. In the benzyl alcohol oxidation, this enhanced mass transfer promotes the oxidation reaction pathway, improving benzaldehyde selectivity and reactant conversion. A selectivity to benzaldehyde that is higher than what is achievable in a conventional stirred glass reactor was observed when operating in the gas-continuous (partially wetted) flow regime, where it reached a maximum of 93%, but the conversion decreased significantly, possibly due to inefficient catalyst utilisation. The conversion could be increased to 81% maintaining the high selectivity by operating at a higher contact time of 530 $g_{cat}\ g_{alc}^{-1}$ s.

The application of response surface methodologies provided a quantitative representation of both conversion and selectivity at different hydrodynamic regimes. The hydrodynamic region leading to the best reaction performance (i.e. high conversion and selectivity) is located in the gas-continuous flow regime, where relatively high gas flow rates in conjunction with moderate liquid flow rates ensure high external mass transfer with a sufficiently wetted catalyst.

Notation

Bo	Bond number
C	conversion, (%)
Ca_L	Capillary number (liquid phase)
C^{MAX}	maximum conversion, (%)

d_p	particle diameter, (m)
f	objective function for the optimisation
f^{MAX}	maximum value of the objective function for the optimisation
g	gravitational acceleration (m/s^2)
G	gas flow rate, (Nml/min)
F_i	i-th experimental factor
F_{PhCHO}	molar flow rate of benzaldehyde, (mol/s)
$F_{PhCH_2OH,0}$	inlet molar flow rate of benzyl alcohol, (mol/s)
F_{PhCH_3}	molar flow rate of toluene, (mol/s)
L	liquid flow rate, (μl/min)
mol_{metal}	moles of metal, (mol)
N	number of experiments
N_F	number of experimental factors
Re_L	Reynolds number (liquid phase)
S	selectivity, (%)
S_{PhCHO}	selectivity to benzaldehyde, (%)
S_{PhCH_3}	selectivity to toluene, (%)
S^{MAX}	maximum selectivity, (%)
TOF_D	disproportionation reaction turnover frequency (s^{-1})
TOF_O	oxidation reaction turnover frequency (s^{-1})
TOF_T	total turnover frequency (s^{-1})
u_G	superficial gas velocity, (m/s)
u_L	superficial liquid velocity, (m/s)
Y	regression model response
Y_0	constant term response surface parameter

Greek symbols

α_i	i-th linear response surface parameter
β_i	i-th quadratic response surface parameter
γ_i	i-th linear interaction response surface parameter
δ_i	i-th quadratic interaction response surface parameter
$\boldsymbol{\theta}$	Set of parameters of the response surface model
λ	dimensionless flow parameter $[(\frac{\rho_G}{\rho_A})(\frac{\rho_L}{\rho_w})]^{0.5}$
μ_L	liquid viscosity, (Pa s)
μ_w	viscosity of water, (Pa s)
ρ_A	density of air, (kg/m^3)
ρ_G	gas density, (kg/m^3)
ρ_L	liquid density, (kg/m^3)
ρ_w	density of water, (kg/m^3)
σ	gas–liquid surface tension, (N/m)
σ_w	water surface tension, (N/m) $\frac{\sigma_w}{\sigma}[(\frac{\mu_L}{\mu_w})(\frac{\rho_w}{\rho_L})^2]^{1/3}$

Acknowledgements

Funding for this work from EPSRC, UK (Grants EP/J017833/1, and EP/J017868/1) is gratefully acknowledged. We also thank the London Centre for Nanotechnology and in particular Steve Etienne for his support in the fabrication of microreactors.

References

Atta, A., Roy, S., Larachi, F., Nigam, K., 2014. Cyclic operation of trickle bed reactors: a review. Chem. Eng. Sci. 115, 205–214.
Al-Rifai, N., Cao, E., Dua, V., Gavriilidis, A., 2013. Microreaction technology aided catalytic process design. Curr. Opin. Chem. Eng. 2 (3), 338–345.
Alsolami, H.B., Berger, J.R., Makkee, M., Moulijn, A.J., 2013. Catalyst performance testing in multiphase systems: implications of using small catalyst particles in hydrodesulfurization. Ind. Eng. Chem. Res. 52, 9069–9085.
Boelhouwer, J.G., Piepers, H.W., Drinkenburg, A.A.H., 2002. Liquid-induced pulsing flow in trickle-bed reactors. Chem. Eng. Sci. 57 (16), 3387–3399.
Box, G.E., Draper, N.R., 1987. Empirical Model Building and Response Surfaces. John Wiley & Sons Inc., New York.
Cao, E., Sankar, M., Nowicka, E., He, Q., Morad, M., Miedziak, P.J., Taylor, S.H., Knight, D.W., Bethell, D., Kiely, C.J., Gavriilidis, A., Hutchings, G.J., 2013. Selective suppression of disproportionation reaction in solvent-less benzyl alcohol oxidation catalysed by supported Au–Pd nanoparticles. Catal. Today 203, 146–152.
Cao, E., Sankar, M., Firth, S., Lam, K.F., Bethell, D., Knight, D.K., Hutchings, G.J., McMillan, P.F., Gavriilidis, A., 2011. Reaction and Raman spectroscopic studies of alcohol oxidation on gold–palladium catalysts in microstructured reactors. Chem. Eng. J. 167 (2–3), 734–743.
Charpentier, J.C., Favier, M., 1975. Some liquid holdup experimental data in trickle-bed reactors for foaming and nonfoaming hydrocarbons. AIChE J. 21, 1213–1218.
Choudhary, V.R., Dumbre, D.K., 2010. Solvent-free selective oxidation of benzyl alcohol to benzaldehyde by tert-butyl hydroperoxide over U_3O_8-supported nano-gold catalysts. Appl. Catal. A: Gen. 375 (2), 252–257.
de Santos, J.M., Melli, T.R., Scriven, L.E., 1991. Mechanics of gas–liquid flow in packed bed contactors. Annu. Rev. Fluid Mech. 23, 233–260.
Doraiswamy, L.K., 2001. Organic Synthesis Engineering. Oxford University Press, Inc., New York.
Enache, D.I., Edwards, J.K., Landon, P., Solsona-Espriu, B., Carley, A.F., Herzing, A.A., Watanabe, M., Kiely, C.J., Knight, D.W., Hutchings, G.J., 2006. Solvent-free oxidation of primary alcohols to aldehydes using Au–Pd/TiO_2 catalyst. Science 311, 362–365.
Faridkhou, A., Larachi, F., 2012. Hydrodynamics of gas–liquid cocurrent flows in micropacked beds – wall visualization study. Ind. Eng. Chem. Res. 51 (50), 16495–16504.
Faridkhou, A., Hamidipour, M., Larachi, F., 2013. Hydrodynamics of gas–liquid micro-fixed beds – measurement approaches and technical challenges. Chem. Eng. J. 223, 425–435.
Faridkhou, A., Larachi, F., 2014. Two-phase flow hydrodynamic study in micro-packed beds – effect of bed geometry and particle size. Chem. Eng. Process.: Process. Intensif. 78, 27–36.
Ferri, D., Mondelli, C., Krumeich, F., Baiker, A., 2006. Discrimination of active palladium sites in catalytic liquid-phase oxidation of benzyl alcohol. J. Phys. Chem. B 110 (46), 22982–22986.
Funk, G.A., Harold, M.P., Ng, L.M., 1991. Experimental study of reaction in a partially wetted catalytic pellet. AIChE J. 37 (2), 202–214.
Goto, S., Smith, J.M., 1975. Trickle-bed reactor performance. Part I. Holdup and mass transfer effects. AIChE J. 21 (4), 706–713.
Hessel, V., Renken, A., Schouten, J., Yoshida, J., 2009. Micro Process Engineering: A Comprehensive Handbook. Wiley-VCH, Weinheim.
Hirose, T., Toda, M., Sato, Y., 1974. Liquid phase mass transfer in packed bed reactor with cocurrent gas–liquid downflow. J. Chem. Eng. Jpn. 7 (3), 187–192.
Hirose, T., Mori, Y., Sato, Y., 1976. Liquid-to-particle mass transfer in fixed bed reactor with cocurrent gas–liquid downflow. J. Chem. Eng. Jpn. 9 (3), 220–225.
Hodoshima, S., Arai, H., Takaiwa, S., Saito, Y., 2003. Catalytic decalin dehydrogenation/naphthalene hydrogenation pair as a hydrogen source for fuel-cell vehicle. Int. J Hydrog. Energy 28, 1255–1262.
Iliuta, I., Hamidipour, M., Schweich, D., Larachi, F., 2012. Two-phase flow in packed-bed microreactors: experiments, model and simulations. Chem. Eng. Sci. 73, 299–313.
Inoue, T., Adachi, J., Ohtaki., K., Lu, M., Murakami, S., Sun, X., Wang, D.F., 2015. Direct hydrogen peroxide synthesis using glass microfabricated reactor – paralleled packed bed operation. Chem. Eng. J. 278, 517–526.
Khadilkar, M.R., Al-Dahhan, M.H., Dudukovic, M.P., 1999. Parametric study of unsteady-state flow modulation in trickle-bed reactors. Chem. Eng. Sci. 54 (13–14), 2585–2595.
Kockmann, N., 2008. Transport Phenomena in Micro Process Engineering. Springer-Verlag, Berlin.
Krishnamurthy, S., Peles, Y., 2007. Gas–liquid two-phase flow across a bank of micropillars. Phys. Fluids 19, 043302.
Lange, R., Gutsche, R., Hanika, J., 1999. Forced periodic operation of a trickle-bed reactor. Chem. Eng. Sci. 54 (13-14), 2569–2573.
Losey, M.W., Schmidt, M.A., Jensen, K.F., 2001. Microfabricated multiphase packed-bed reactors: characterization of mass transfer and reactions. Ind. Eng. Chem. Res. 40 (12), 2555–2562.
Moulijn, J., Makkee, M., Berger, R., 2016. Catalyst testing in multiphase micro-packed-bed reactors; criterion for radial mass transport. Catal. Today 259, 354–359.
Meenakshisundaram, S., Nowicka, E., Miedziak, P.J., Brett, G.L., Jenkins, R.L., Dimitratos, N., Taylor, S.H., Knight, D.W., Bethell, D., Hutchings, G.J., 2010. Oxidation of alcohols using supported gold and gold–palladium nanoparticles. Faraday Discuss. 145, 341–356.
Montgomery, D., 2005. Design and Analysis of Experiments. John Wiley & Sons Inc, Hoboken.
Orgill, J.J., Atiyeh, H.K., Devarapalli, M., Phillips, J.R., Lewis, R.S., Huhnke, R.L., 2013. A comparison of mass transfer coefficients between trickle-bed, hollow fiber membrane and stirred tank reactors. Bioresour. Technol. 133, 340–346.
Ranade, V., Chaudhari, R., Gunjal, P., 2011. Trickle Bed Reactors: Reactor Engineering & Applications. Elsevier, Oxford.
Sankar, M., Nowicka, E., Tiruvalam, R., He, Q., Taylor, S.H., Kiely, C.J., Bethell, D., Knight, D.W., Hutchings, G.J., 2011. Controlling the duality of the mechanism in liquid-phase oxidation of benzyl alcohol catalysed by supported Au–Pd nanoparticles. Chem. Eur. J 17, 6524–6532.
Sankar, M., He, Q.F., Morad, M.F., Pritchard, J.F., Freakley, S.J., Edwards, J.K., Taylor, S., Morgan, D.J., Carley, A.F., Knight, D.W., Kiely, C.J., Hutchings, G.J., 2012. Synthesis of stable ligand-free gold–palladium nanoparticles using a simple excess anion method. ACS Nano 6 (8), 6600–6613.

Shao, N., Gavriilidis, A., Angeli, A., 2009. Flow regimes for adiabatic gas–liquid flow in microchannels. Chem. Eng. Sci. 64 (11), 2749–2761.
van Herk, D., Kreutzer, M.T., Makkee, M., Moulijn, J.A., 2005. Scaling down trickle bed reactors. Catal. Today 106 (1–4), 227–232.
Wilhite, B.A., Wu, R., Huang, X., McCready, M.J., Varma, A., 2001. Enhancing performance of three-phase catalytic packed-bed reactors. AIChE J. 47 (11), 2548–2556.
Wilhite, B.A., Huang, X., McCready, M.J., Varma, A., 2003. Effects of induced pulsing flow on trickle-bed reactor performance. Ind. Eng. Chem. Res. 42 (10), 2139–2145.
Xiao, Q., Cheng, Z.M., Jiang, Z.X., Anter, A.M., Yuan, W.K., 2001. Hydrodynamic behavior of a trickle bed reactor under forced pulsing flow. Chem. Eng. Sci. 56 (3), 1189–1195.
Yamaguchi, K., Mizuno, N., 2002. Supported ruthenium catalyst for the heterogeneous oxidation of alcohols with molecular oxygen. Angew. Chem. 114 (23), 4720–4724.
Yang, M.-C., Cussler, E.L., 1987. A hollow-fiber trickle bed reactor. AIChE J. 33 (10), 1754–1756.